Locating Faults Before the Breaker Opens – Adaptive Autoreclosing Based on the Location of the Fault

Bogdan Kasztenny, Armando Guzmán, Mangapathirao V. Mynam, and Titiksha Joshi
Schweitzer Engineering Laboratories, Inc.

This paper was presented at the 71st Annual Conference for Protective Relay Engineers and can be accessed at: https://doi.org/10.1109/CPRE.2018.8349806.

For the complete history of this paper, refer to the next page.

Revised edition released October 2019

Previously presented at the
9th Annual Protection, Automation and Control World Conference, June 2018,
72nd Annual Georgia Tech Protective Relaying Conference, May 2018,
71st Annual Conference for Protective Relay Engineers, March 2018, and
7th International Conference on Power System Protection and Automation, February 2018

Previously published in
Locating Faults and Protecting Lines at the Speed of Light: Time-Domain Principles Applied, 2018, and
Wide-Area Protection and Control Systems: A Collection of Technical Papers Representing Modern Solutions, 2017

Originally presented at the
44th Annual Western Protective Relay Conference, October 2017

Locating Faults Before the Breaker Opens – Adaptive Autoreclosing Based on the Location of the Fault

Bogdan Kasztenny, Armando Guzmán, Mangapathirao V. Mynam, and Titiksha Joshi,
Schweitzer Engineering Laboratories, Inc.

***Abstract*—This paper reviews technical, safety, and economical merits of adaptive autoreclosing based on fault location calculated in real time. These applications include preventing reclosing for faults on cable sections of hybrid lines comprising overhead and cable sections, faults located close to large generating stations, faults on line sections crossing densely populated areas or fire-prone terrain, or faults on line sections near airports that receive small airplanes. The paper explains principles of fault locating based on traveling waves and introduces an adaptive autoreclosing control logic to allow or cancel reclosing based on the location of the fault. The paper includes examples that explain and illustrate these principles. The paper also describes several methods of using operational data—internal and external faults as well as switching events—to further improve the fault-locating accuracy of a commissioned fault locator.**

I. Introduction

Historically, fault location information has been provided to a line maintenance crew just in time for them to inspect and repair a line after a permanent fault. Today, with impedance-based fault locating widely available in microprocessor-based protective relays integrated with SCADA, system operators have access to fault location information within seconds [1]. A system operator can learn the fault type and location at the same time he or she realizes a given line has been tripped and locked out. To support this timely assistance for system operators, line protective relays calculate and communicate fault location and fault type within several seconds.

The next step in the practice of fault locating embedded in protective relays is to provide the fault type and accurate fault location information within milliseconds, in order to facilitate control functions such as adaptive control of autoreclosing.

Today, a typical autoreclosing logic may use a number of reclosing attempts (shots) with different dead-time intervals for the successive reclosing attempts. Both the shot count and the dead-time intervals may vary depending on whether the relay tripped a single pole or three poles of a circuit breaker. In general, when tripping a single pole of the circuit breaker, you may want to allow more time for the secondary arc extinction. You may also want to allow more time for ionized air to recover its insulation capability after each unsuccessful reclose attempt. In three-pole tripping applications, autoreclosing logic very rarely responds to the fault type.

Today, impedance-based fault locators, especially the single-ended ones, do not guarantee enough accuracy under all fault conditions to support controlling the reclosing logic based on the fault location. Also, today's relays do not typically calculate fault location quickly enough to use it for adaptive control of autoreclosing.

This paper reviews technical, safety, and economical merits of adaptive autoreclosing based on fault location, and it presents a method for accurate fault locating using traveling waves (TWs) from both terminals of the line to facilitate such location-dependent "surgical autoreclosing." The paper illustrates the new principles with simulations and test results from a line relay that provides the first-ever adaptive autoreclosing logic controlled by fault location.

The paper also describes several methods of using operational data—internal and external faults as well as switching events—to further improve the fault-locating accuracy of a commissioned fault locator. These methods allow us to improve the accuracy of fault locator settings as well as create more accurate mapping between the distance to the fault that the fault locator reports and the actual location of the tower with the fault.

II. Applications and Benefits of Autoreclosing Controlled by Fault Location

A. Hybrid Lines With Overhead Line Sections and Underground Cable Sections

Hybrid lines comprising overhead line sections and underground cable sections are becoming more common, especially in urban areas. The underground cable sections are typically more expensive and are only used to cross densely populated areas, airports, highways, or terrain where obtaining an above-the-ground right-of-way is difficult for a variety of reasons, including environmental and aesthetic constraints. Also, the per-mile capacitive charging current drawn by cable sections is considerably higher than for an overhead line section. As a result of their higher per-mile cost and charging current, the underground cable sections are typically considerably shorter than the overhead line sections. A hybrid line can have more than one underground cable section.

Many faults on overhead lines are temporary faults, allowing for a high rate of successful autoreclosing [2]. After a circuit breaker trips a temporary fault on an overhead line, the fault-ionized air is replaced with fresh air during the autoreclosing dead-time. With this regenerated insulation, the line continues

to operate normally after reclosing, as long as the insulators have not been damaged by the fault. In contrast, all faults on underground cables are permanent faults. Precursors to faults (incipient faults) are transient in nature, but once the solid cable insulation is damaged, it will not restore itself. As a result, autoreclosing for faults on cables is counterproductive; it further damages the cable causing longer and more expensive repair.

Ideally, you would prefer to allow autoreclosing on overhead line sections and to block autoreclosing on underground cable sections of a hybrid line. In single-pole tripping applications, a single-pole trip for a fault on a cable section should be converted into a three-pole trip, and the autoreclosing scheme should not reclose for that fault.

Today, there are no economical solutions to this operational challenge. Reference [3] proposes installing current transformers (CTs) at each transition between a cable and an overhead line section and obtaining current measurement via a fiber-optic connection to one of the line terminals. Using the current measurement at each transition point, the logic implements a differential zone for each cable section and sends a block command to the autoreclosing device if the fault is located in one of the cable sections (in one of the differential zones). In order to avoid electronics and having to bring auxiliary control power to the CTs located along the line, solution [3] uses a piezoelectric element to convert the current signal into a mechanical displacement signal. Further, it uses a Bragg-effect fiber-optic filter to sense the mechanical displacement remotely with the laser source and the associated sensing electronics located at the main line terminal. This solution is still under development and has the drawback of requiring CTs at each transition point and fiber-optic cables from each of these CTs to the main line terminal where the autoreclosing device is located.

Another solution to the adaptive control of autoreclosing of hybrid lines is to use fault location information. However, impedance-based fault-locating methods have limited accuracy because of a number of factors we explain in Section III.A. As a result, impedance-based fault-locating methods are not accurate enough for autoreclosing control applications. In hybrid lines with several short cable sections, the fault location information would have to be available with accuracy of a small fraction of the shortest cable section length.

This paper shows that the double-ended TW-based fault-locating method with correction for line nonhomogeneity solves both problems. It provides an accurate fault location to allow or block autoreclosing for faults on overhead or cable sections, accordingly and to accelerate line repairs after permanent faults by reducing the fault search time.

B. Lines Terminating at Large Generating Stations

Reclosing for a permanent fault near a generating station has adverse effects on generators and turbines [2] [4]. Large transient torque created when closing on a high-current fault stresses the generator shaft, turbine shaft, their bearings, and other mechanical components of the unit. The best reclosing practice for these lines is to test the line from the remote line terminal (the terminal away from the generating station) and then reclose the circuit breaker at the generator terminal with synchronism-check supervision [2]. Some lines, however, have generating stations close to both terminals. Inhibiting autoreclosing for high-current close-in or three-phase faults but allowing reclosing for lower-current remote faults reduces the mechanical stress on the generator and the turbine [2]. One potential solution when deciding to allow or block autoreclosing is to use the magnitude of the short-circuit current. The magnitude of the fault current is not, however, a reliable predictor of the current during autoreclosing for the following reasons:

- An initial single-line-to-ground fault may evolve into a double-phase-to-ground or a three-phase fault after the circuit breaker recloses.
- An initial resistive fault may evolve into a bolted fault after the circuit breaker recloses.
- The magnitude of the line current depends on how many generating units near the line terminal are in service at a given time.

As a result, using the initial fault current, we may considerably underestimate the current during subsequent reclosing. Also, the current-based autoreclosing control logic may need to constantly adapt, via settings groups, to the number of generating units in service.

Fault location is a more reliable indication of the worst-case impact of reclosing onto a permanent fault. One should assume a bolted three-phase fault when determining the range of fault locations for which to inhibit autoreclosing. For example, a line with generation near both terminals can be reclosed from the terminal away from the fault location.

In addition to the traditional factors limiting accuracy of the impedance-based fault-locating methods [1], they may exhibit an additional error when applied near generating stations because of the transient and subtransient decaying ac components in the fault current. Using TW-based fault locating with accuracy on the order of a single tower span allows location-based control of autoreclosing for lines near generating stations.

C. Lines With Public Safety Concerns

Reclosing onto a permanent fault creates a second high-energy event at the fault location, in addition to the initial fault. There are several situations when it may be beneficial to avoid reclosing. They include:

- Highly populated areas, such as subtransmission lines sharing the right-of-way with roads or even residential streets. Not reclosing for fault locations where humans are likely to be present improves safety.
- Airports, especially regional airports receiving small airplanes operated by amateur pilots. Not reclosing for fault locations where a small airplane may have inadvertently flown into the line is beneficial.

- Fire-prone terrain such as forests or bush areas, especially in very dry climates or seasons. Not reclosing for faults on these fire-prone stretches of the line reduces the potential of starting large and expensive wildfires.

In some applications, utilities can block autoreclosing for certain fault locations on a seasonal or temporary basis.

D. Other Applications

Location-dependent autoreclosing may have other applications. For example, the two autoreclosing schemes at both ends of the line may exchange their roles based on the location of the fault. The terminal farther away from the fault may close first, and for a temporary fault, the other terminal follows.

In another application, a utility may see a very low autoreclosing success rate for faults on certain sections of the line depending on construction or surroundings of these sections. Location-dependent autoreclosing offers an option to block reclosing for these low-success-rate sections, while allowing reclosing for faults elsewhere on the line.

III. Fault Locating on Hybrid Lines With Overhead Line Sections and Underground Cable Sections

A. Limitations of Impedance-Based Methods

Impedance-based fault-locating methods using the total line impedance value of the hybrid line face the following challenges [5]:

- The positive-sequence impedance per mile is very different for the overhead sections and cable sections.
- The Z_0/Z_1 ratio is very different for the overhead sections and cable sections. This puts the single-ended methods at a considerable disadvantage for ground faults—the same apparent impedance is possible for multiple fault locations. Double-ended fault locators [6] can better resolve this problem by using negative-sequence voltage and current, identifying the faulted section using impedances of each section and calculating the accurate fault location for the faulted section.
- The zero-sequence impedance for cable sections is a nonlinear function of the fault current [7]. This challenges both the single- and double-ended impedance-based methods that use zero-sequence measurements—the zero-sequence network may have a slightly different impedance depending on how much short-circuit current flows in the cable.
- The zero-sequence impedance for cable sections is uncertain and it depends on the grounding and shielding methods, other cables and pipes buried in the same right of way, rail tracks, or other conductive paths in the vicinity. The inaccuracy and variability in the zero-sequence impedance considerably challenges the single-ended fault-locating methods for ground faults. The double-ended methods may use negative-sequence measurements, and therefore they are not impacted by the zero-sequence impedance errors.

In addition, the following common factors affect the accuracy of impedance-based methods:

- Ratio errors in CTs and voltage transformers (VTs).
- Phasor measurement errors in the fault-locating device, including errors caused by transients when using fast relays and circuit breakers.
- Finite accuracy of impedance and line length data, including the weather and seasonal variability in the zero-sequence line impedance.
- Impact of fault resistance on single-ended methods.
- Impact of changes in fault resistance on single-ended methods and to some degree on double-ended methods.
- Impact of the line charging current.
- Finite accuracy of synchronizing sampling clocks between the fault locators at the two line terminals in double-ended methods.

As a result of the general accuracy-limiting factors and accuracy-limiting factors specific to cables and hybrid lines, the expected fault-locating accuracy of impedance-based methods in cables or hybrid lines can be on the order of 10 percent or worse. A conservative approach to controlling autoreclosing for hybrid lines would be to set the blocking intervals with margins to guarantee blocking for faults on cables or at junction points despite the fault-locating error. This method would effectively allow reclosing for a relatively small proportion of the total overhead line length. For example, consider a hybrid line with two cable sections along the line and away from the main line terminals totaling 30 percent of the line length. The 10 percent margins on each end of the two cable sections add up to 40 percent of the line length, allowing autoreclosing for 70 – 40 = 30 percent of the line length, i.e., less than half the length of the overhead line.

B. Double-Ended TW-Based Fault-Locating Principle

Fig. 1 shows a Bewley diagram for a fault at location F on a line of length LL. The fault is M (km or mi) away from the local terminal (S) and LL – M (km or mi) away from the remote terminal (R). The TW propagation velocity (PV) for the line is the ratio of the total line length (LL) and the TW line propagation time (TWLPT) settings of the fault locator:

$$\mathrm{PV} = \frac{\mathrm{LL}}{\mathrm{TWLPT}} \tag{1}$$

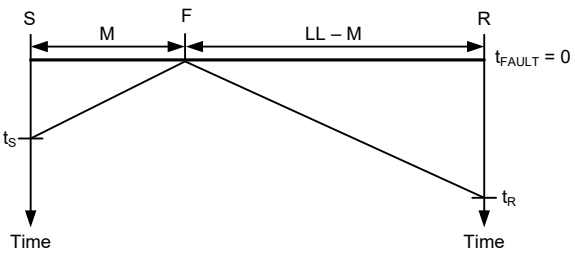

Fig. 1. Bewley diagram explaining double-ended TW-based fault locating.

The first current TW arrives at Terminal S at:

$$t_S = \frac{M}{PV} \tag{2}$$

The first current TW arrives at Terminal R at:

$$t_R = \frac{LL - M}{PV} \tag{3}$$

Solving (2) and (3) for the fault location, M, and factoring in (1) for the propagation velocity, we obtain the following fault-locating equation:

$$M = \frac{LL}{2} \cdot \left(1 + \frac{t_S - t_R}{TWLPT}\right) \tag{4}$$

Some advanced double-ended fault locators [8] may compensate for the CT cable delays at both line terminals. The CT cable delay (TWCPT) is a setting. The fault-locating algorithm backdates the TW time stamps by the cable delays at both terminals of the line as follows:

$$M = \frac{LL}{2} \cdot \left(1 + \frac{(t_S - TWCPT_S) - (t_R - TWCPT_R)}{TWLPT}\right) \tag{5a}$$

To better understand the impact of CT cable delays, let us separate the time stamps (measurements) from the cable delays (settings) in (5a) as follows:

$$M = \frac{LL}{2} \cdot \left(1 + \frac{(t_S - t_R) - (TWCPT_S - TWCPT_R)}{TWLPT}\right) \tag{5b}$$

Equation (5b) signifies that the difference in the CT cable propagation delays, not the individual delays, impacts the double-ended TW-based fault-locating method. The cable compensation becomes marginally important if the two CT cable delays are similar ($TWCPT_S \cong TWCPT_R$).

The fault-locating method (4) measures current TWs by using a differentiator-smoother filter [9]. A practical implementation [8] of this method applies the differentiator-smoother filter to current samples taken every microsecond. The method further incorporates a time-stamping algorithm that uses interpolation to find the time of the peak for the output of the differentiator-smoother filter. This interpolation provides a time-stamping accuracy of approximately 0.1 μs, i.e., about ten times better than the sampling interval.

Traveling waves contain aerial and ground modes [9]. The ground mode exhibits larger dispersion, resulting in less accurate time stamping than when using aerial modes. Therefore, the fault-locating method (4) uses the aerial mode (alpha or beta) appropriate for a given fault type. One practical fault locator [8] selects the mode with the highest magnitude from among the three alpha and three beta aerial modes when calculating time stamps. Subsection III.E provides more information on time stamping and mode selection for applying the fault-locating method (4) to cables and hybrid lines.

The double-ended TW-based fault-locating method (4) is simple, yet very accurate. It requires identifying and time-stamping only the very first TWs at both line terminals. Not having to isolate and identify the origin of any subsequent TWs is a great advantage of this fault-locating method [9] compared with the single-ended method. Because (4) is a double-ended method, it requires the TW-based fault-locating devices at both line terminals to be synchronized so that the TW arrival times at both line terminals are captured with the same time reference. The synchronization is typically achieved using satellite-synchronized clocks [10] or using a direct point-to-point fiber-optic channel between the devices [8].

Equation (4) uses two static data items (settings) and two time stamps (measurements). Enhanced method (5) uses two more settings for even better accuracy. We offer the following accuracy analysis of the fault-locating methods (4) and (5) with respect to their settings and the measurements:

- 1 percent of error in the LL setting results in 1 percent of error in the fault location.
- 1 μs of error in the TWLPT setting results in a fault-locating error of as much as 150 m (500 ft) for overhead lines and as much as 75 m (250 ft) for underground cables.
- 0.1 μs of error in the TWCPT setting results in a fault-locating error of about 15 m (50 ft) for overhead lines and about 7.5 m (25 ft) for underground cables.
- 0.1 μs of error in device time stamping results in a fault-locating error of about 15 m (50 ft) for overhead lines and about 7.5 m (25 ft) for underground cables.

For overhead line sections, expect line sag of up to about 0.3 percent of the line length. The sag changes with ambient temperature and line loading, resulting in line length changes of up to a fraction of 0.3 percent. As a result, you may expect an extra fault-locating error of a fraction of 0.3 percent. Note that for a 161 km (100 mi) line, 0.3 percent of length is about 480 m (1600 ft) or about 1.5 tower spans.

Minimize errors in the TWLPT setting by measuring the TW line propagation time during commissioning of the fault locator. To do this, energize the line and capture the round-trip time of the TWs launched by the closure of the local circuit breaker and reflected back from the opened remote circuit breaker (see Section IV for more details).

Improve line length data (LL setting) accuracy by correlating reported fault locations with actual locations found by your line crews (see the Appendix for more details).

Approximate the CT cable lengths and calculate the corresponding TWCPT settings to account for the TW travel time between the CTs and the fault-locating device. You can either use the cable datasheet or perform a cable propagation time measurement using time-domain reflectometry (TDR).

When using satellite clocks for time synchronization in TW-based fault locators, such as in solution [10], apply high accuracy clocks and use antenna cable delay compensation available in some advanced satellite clocks.

The double-ended TW-based fault-locating method (4) has a field-proven track record with reported accuracy within one tower span (300 m or 1000 ft) on average [9]. When tested

under ideal conditions, the double-ended TW-based fault-locating method (4) implemented on a hardware platform [8] yields a 90th percentile error considerably below 20 m (66 ft) and a median error less than 10 m (33 ft).

C. Double-Ended TW-Based Fault Locating for Hybrid Lines

Consider the hybrid line depicted in Fig. 2, comprising two overhead line sections, 1 and 3, and one underground cable section, 2. The overhead section lengths are LL_1 and LL_3 and the cable section length is LL_2. The TW line propagation times for the overhead line sections are $TWLPT_1$ and $TWLPT_3$ and the TW line propagation time for the cable section is $TWLPT_2$.

Expect different propagation velocities for the overhead and cable sections as follows:

$$\frac{LL_1}{TWLPT_1} \cong \frac{LL_3}{TWLPT_3} \gg \frac{LL_2}{TWLPT_2} \tag{6}$$

For example, the propagation velocity for the overhead line sections can be approximately 98 percent of the speed of light in free space, while the propagation velocity for the cable section can be as low as 50 percent of the speed of light in free space.

The line of Fig. 2a can be conveniently depicted as a piece-wise linear characteristic representing the relationship between the distance-to-fault and the TW line propagation time to the fault location (Fig. 2b).

Let us denote the total line length as LL:

$$LL = LL_1 + LL_2 + LL_3 \tag{7}$$

and the total TW line propagation time as TWLPT:

$$TWLPT = TWLPT_1 + TWLPT_2 + TWLPT_3 \tag{8}$$

For any fault location (F), if one line terminal measures the TW arrival time as t_S, the other terminal measures the TW arrival time as $t_R = TWLPT - t_S$ (see Fig. 2b).

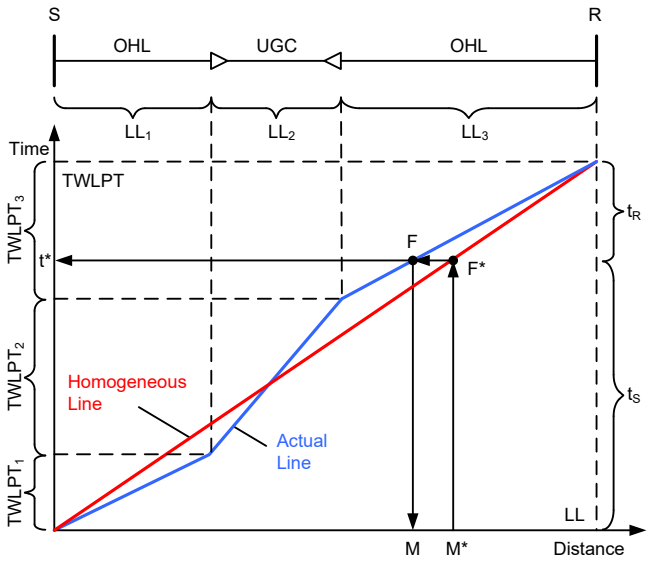

Fig. 2. Sample hybrid line with two overhead sections and one cable section (a) and its distance-propagation time characteristic (b).

Assume we use the fault-locating method (4) neglecting the line nonhomogeneity, i.e., we use (4) with the total line length (7) and the total TW line propagation time (8) as settings and the TW arrival time difference ($t_S - t_R$) as the measurement. If so, we obtain a fault location (M^*) as illustrated in Fig. 2. This fault location is not accurate and represents a fictitious fault (F^*) shown in Fig. 2.

Note, however, that the TW arrival time difference ($t_S - t_R$) applies to the actual fault (F) and its true location (M). Therefore, we simply correct the result (M^*) by projecting it from the straight line characteristic representing a homogeneous power line in Fig. 2, to the actual line characteristic representing the hybrid line ($F^* \rightarrow F$ in Fig. 2b).

We summarize our double-ended TW-based fault-locating method for hybrid (nonhomogeneous) lines as follows:

Step 1. Calculate the fault location (M^*) with (4) as if the line were homogeneous, i.e., using the total line length and the total TW line propagation time.

Step 2. Calculate the propagation time (t^*) corresponding to the fault location (M^*) assuming the line is homogeneous, i.e., using the straight line between the origin and the point defined by the total line length and the total TW line propagation time.

Step 3. Calculate the actual fault location (M) corresponding to the propagation time (t^*) using the nonhomogeneity distance-propagation time characteristic of the line.

Fig. 3 illustrates the above three-step process.

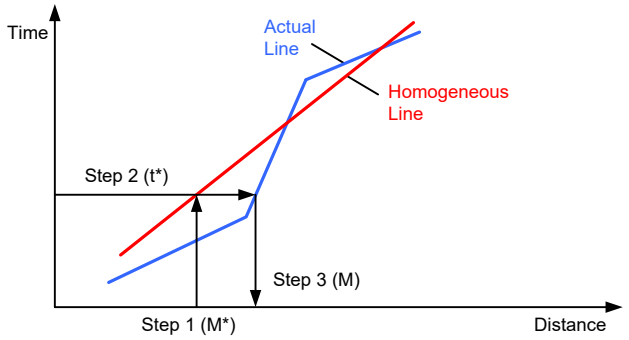

Fig. 3. Illustration of the three-step method to calculate double-ended TW-based fault location for nonhomogeneous lines.

D. Numerical Example

Consider the hybrid 138 kV line depicted in Fig. 2a with the overhead line sections and underground cable section data given in Table I.

TABLE I
HYBRID LINE DATA USED IN THE NUMERICAL EXAMPLE

Section	Type	Length (mi)	Propagation Time (μs)
1	Overhead	20.00	107.50
2	Cable	8.00	81.50
3	Overhead	10.00	53.75
Total	Hybrid	38.00	242.75

We modeled this line with an electromagnetic transient program using data for a sample 138 kV overhead line and a 138 kV single-core coaxial underground cable.

Fig. 4 shows the distance-propagation time characteristic of the line as plotted in the PC setup software for the fault locator [8]. The origin represents Terminal S of the line.

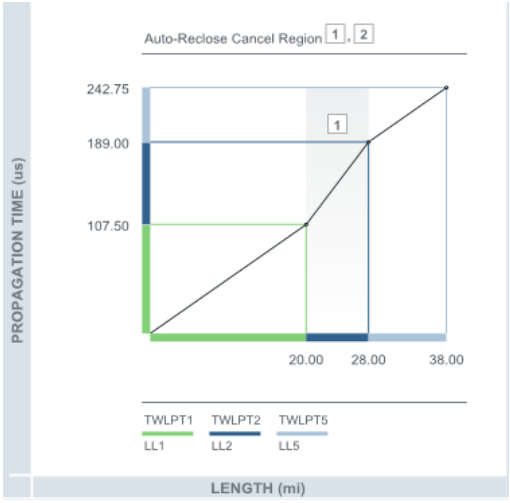

Fig. 4. Distance-propagation time characteristic of the sample line (Table I).

1) Example 1. Fault on the Overhead Section

An AG fault occurred on Section 1 of the overhead line, 15 mi from Terminal S. Fig. 5 shows the voltages and currents at Terminals S and R. Fig. 6 shows the terminal currents at the time of arrival of the first TWs. Fig. 7 shows the alpha aerial current referenced to Phase A at the output of the differentiator-smoother filter used to extract the current TWs from the measured currents.

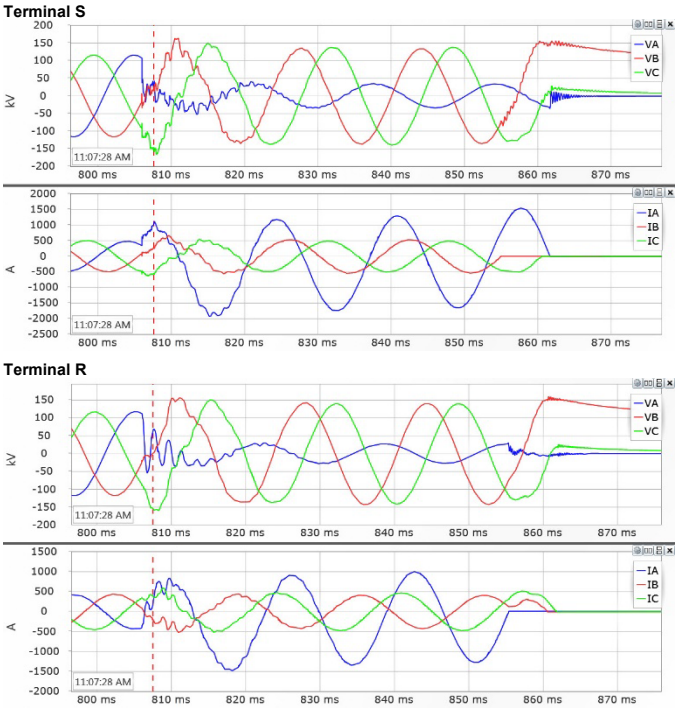

Fig. 5. Example 1: Voltages and currents at Terminals S and R.

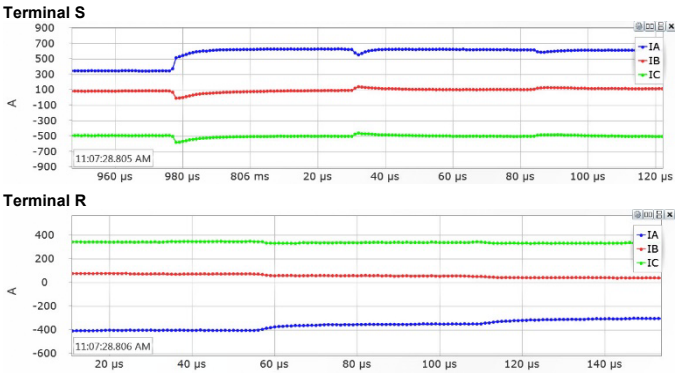

Fig. 6. Example 1: Currents at Terminals S and R on the time scale selected to show the first TWs arriving at the line terminals.

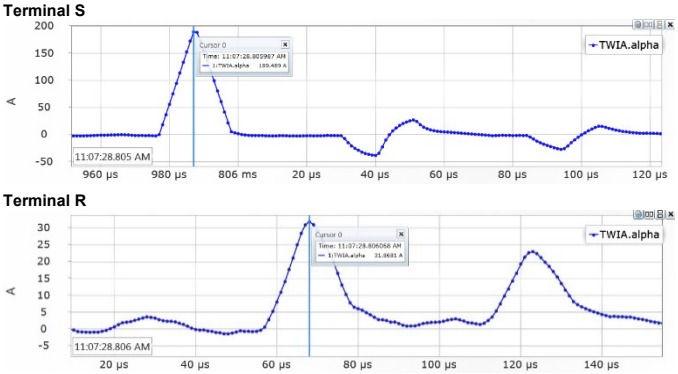

Fig. 7. Example 1: Very first current TWs at Terminals S and R.

The time-stamping algorithm [8] calculates the following TW arrival times at Terminals S and R for the TWs shown in Fig. 7 (the figure only shows rough time stamps with a 1 µs resolution):

$$t_S = 805{,}987.549\ \mu s \text{ and } t_R = 806{,}068.341\ \mu s$$

Using (4), we calculate the raw fault location as follows (Step 1):

$$M^* = \frac{38}{2} \cdot \left(1 + \frac{5{,}987.549 - 6{,}068.341}{242.75}\right) = 12.676 \text{ mi}$$

Assuming a homogeneous line, we obtain the following TW line propagation time from Terminal S to the fault (Step 2):

$$t^* = 12.676 \cdot \frac{242.75}{38} = 80.976\ \mu s$$

Using the nonhomogeneity characteristic from Fig. 4, we obtain the true fault location (Step 3):

$$80.976\ \mu s \rightarrow 15.066 \text{ mi}$$

The 0.066 mi error is about 350 ft, or about one-third of a tower span.

We can double-check the above result to better illustrate the principle. If the fault is located at 15.066 mi, the TW line propagation time to Terminal S is:

$$15.066 \cdot \frac{107.5}{20} = 80.980\ \mu s$$

At the same time, the TW line propagation time to Terminal R is:

$$(20 - 15.066) \cdot \frac{107.5}{20} + 81.50 + 53.75 = 161.770\ \mu s$$

The difference in the TW arrival times is therefore:

$$80.980 - 161.770 = -80.790 \text{ µs}$$

The above value is the difference between the TW arrival times that the fault locator calculated:

$$805{,}987.549 - 806{,}068.341 = -80.792 \text{ µs}$$

The above expression confirms that the fault is truly 15 mi from Terminal S (the 350 ft error notwithstanding).

2) Example 2. Fault on the Underground Section

A BG fault occurred on Section 2 (underground cable), 23 mi from Terminal S or 3 mi from the transition point between Section 1 and Section 2. Fig. 8 shows the voltages and currents at Terminals S and R. Fig. 9 shows the terminal currents at the time of arrival of the first TWs. Fig. 10 shows the alpha aerial current referenced to Phase B at the output of the differentiator-smoother filter used to extract the current TWs from the measured currents.

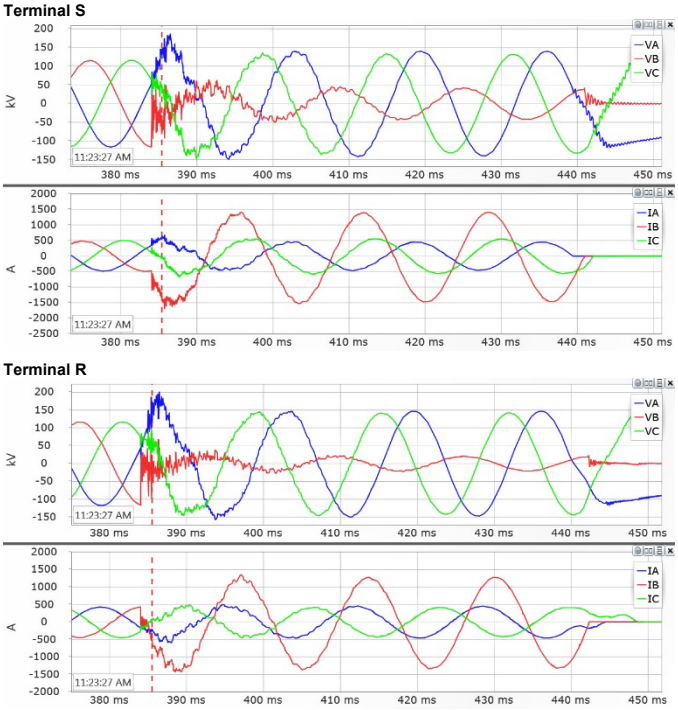

Fig. 8. Example 2: Voltages and currents at Terminals S and R.

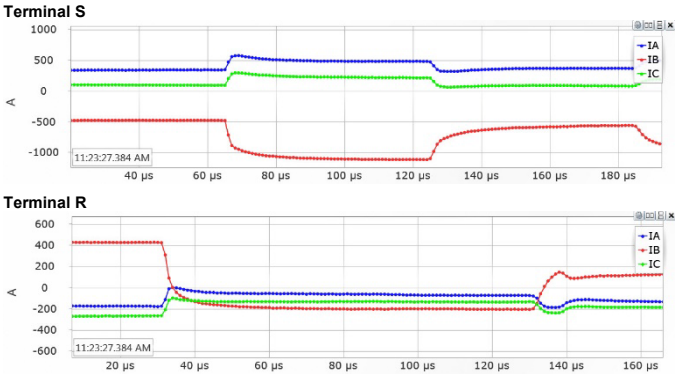

Fig. 9. Example 2: Currents at Terminals S and R on the time scale selected to show the first TWs arriving at the line terminals.

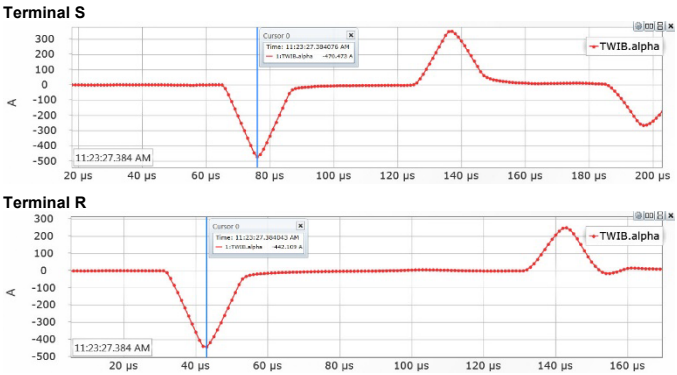

Fig. 10. Example 2: Very first current TWs at Terminals S and R.

The time-stamping algorithm [8] calculates the following TW arrival times at Terminals S and R for the TWs shown in Fig. 10 (the figure only shows rough time stamps with a 1 µs resolution):

$$t_S = 384{,}076.341 \text{ µs and } t_R = 384{,}042.813 \text{ µs}$$

Using (4), we calculate the raw fault location as follows (Step 1):

$$M^* = \frac{38}{2} \cdot \left(1 + \frac{76.341 - 42.813}{242.75}\right) = 21.624 \text{ mi}$$

Assuming a homogeneous line, we obtain the following TW line propagation time from Terminal S to the fault (Step 2):

$$t^* = 21.624 \cdot \frac{242.75}{38} = 138.137 \text{ µs}$$

Using the nonhomogeneity characteristic from Fig. 4, we obtain the true fault location (Step 3):

$$138.137 \text{ µs} \rightarrow 23.008 \text{ mi}$$

The 0.008 mi error is about 42 ft.

We can double-check the above result to better illustrate the principle. If the fault is located at 23.008 mi, the TW line propagation time to Terminal S is:

$$107.50 + 3.008 \cdot \frac{81.50}{8} = 138.144 \text{ µs}$$

At the same time, the TW line propagation time to Terminal R is:

$$(8 - 3.008) \cdot \frac{81.50}{8} + 53.75 = 104.606 \text{ µs}$$

The difference in the TW arrival times is therefore:

$$138.144 - 104.606 = 33.538 \text{ µs}$$

The above value is the difference between the TW arrival times that the fault locator calculated:

$$384{,}076.341 - 384{,}042.813 = 33.528 \text{ µs}$$

The above expression confirms that the fault is truly 3 mi from the transition between Sections 1 and 2 of the hybrid line (the 42 ft error notwithstanding).

E. Signal Processing and Mode Selection

Underground cables exhibit much higher TW dispersion and attenuation than overhead lines.

From the signal processing point of view, dispersion refers to a phenomenon where a TW launched as a step change (an ideal wave) exhibits a ramp-up time that increases with the distance traveled by the wave (Fig. 11). In order to accurately and consistently capture the TW arrival time, the time-stamping algorithm [8] uses an adequately long data window in the differentiator-smoother filter. The time of the peak of the output from the differentiator-smoother consistently represents the midpoint on the TW ramp.

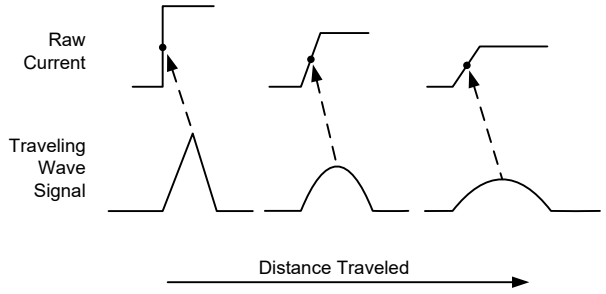

Fig. 11. Explanation of dispersion and its impact on time stamping.

Attenuation refers to a phenomenon where the magnitude of a TW decreases as the TW travels along the line (Fig. 11). In order to capture small TWs, a practical fault locator uses an 18-bit analog-to-digital converter [8].

Selecting a mode signal for time stamping is another application consideration when locating faults on underground cables or hybrid lines with a considerable total cable section length. Aerial modes account for coupling between the phase conductors, and as such they apply to lines in which such a coupling takes place. Single-phase cables with individual shields do not exhibit coupling between the conductors of a three-phase cable section. Applying aerial modes on such cables may reduce the signal level, lowering the time-stamping accuracy and consequently, the fault-locating accuracy.

In order to address this challenge, the fault-locating solution [8] allows selecting either aerial or phase signals for time stamping. Use aerial TWs for time stamping if one of the following is true:

- The hybrid line has overhead sections connected to both line terminals. These overhead sections will allow the TWs to couple before they reach the line terminals resulting in the typical TW patterns seen in a purely overhead line.
- The hybrid line has relatively short cable sections.

Otherwise consider using phase TWs for time stamping.

F. Loss of TW Signal Level Due to Reflections

Transitions between overhead line sections and underground cable sections cause TW reflection because of the very different characteristic impedance values of overhead lines (approximately 300–400 Ω) and underground cables (approximately 50–70 Ω).

A current TW *reflection coefficient* defines the magnitude of the current TW reflected from a discontinuity between line sections with Z_{C1} and Z_{C2} characteristic impedances. Assuming an incident TW traveled along the line section with Z_{C1} characteristic impedance, the TW reflected from the transition to the section with Z_{C2} characteristic impedance is:

$$R_I = \frac{Z_{C1} - Z_{C2}}{Z_{C1} + Z_{C2}} \tag{9}$$

A current TW *transmission coefficient* defines the magnitude of the current TW transmitted through a discontinuity between line sections with Z_{C1} and Z_{C2} characteristic impedances. Assuming an incident TW traveled along the line section with Z_{C1} characteristic impedance, the TW transmitted into the line section with Z_{C2} characteristic impedance is:

$$T_I = \frac{2 \cdot Z_{C1}}{Z_{C1} + Z_{C2}} \tag{10}$$

1) TW Transition From an Overhead Line Section to an Underground Cable Section

Assume Z_{C1} = 300 Ω and Z_{C2} = 70 Ω. The reflection coefficient given by (9) is 0.62, and the transmission coefficient given by (10) is 1.62.

Transitioning from an overhead line section to an underground cable section boosts the incident TW when it enters the cable section (1.62 multiplier in our example). At the same time, a considerably large TW reflects from the transition point (62 percent of the incident TW), allowing us to identify reflections from that discontinuity.

2) TW Transition From an Underground Cable Section to an Overhead Line Section

Assume Z_{C1} = 70 Ω and Z_{C2} = 300 Ω. The reflection coefficient given by (9) is –0.62, and the transmission coefficient given by (10) is 0.38.

Transitioning from an underground cable section to an overhead line section considerably reduces the magnitude of the transmitted TW when it enters the overhead section (0.38 multiplier in our example). Still, a considerably large TW reflects from the transition point (62 percent of the incident TW, with opposite polarity), allowing us to identify reflections from that discontinuity.

It is important to remember that for a fault occurring at the same voltage point-on-wave, the magnitude of the incident current TW for a fault on a cable section is 5–8 times higher than for a fault on an overhead section, because the cable characteristic impedance is 5–8 times lower than that of an overhead line. Transitioning from an underground cable section to an overhead line section greatly reduces the TW magnitude. The current TW for a cable fault is, however, much higher, and even when reduced during transition from the cable section to an adjacent overhead section, it is still similar to the current TW for a fault on the overhead line section.

3) Numerical Example 1

Assume a fault on Section 1 of the hybrid line in Table I. Assume further, a bolted fault occurred when the voltage was at 150 kV peak, launching an incident current TW of 150 kV / 300 Ω = 500 A. Fig. 12 shows the incident and reflected TWs for this fault neglecting any attenuation and dispersion. Notice that the sum of the incident and reflected current TWs to the left of a transition point is equal to the sum of the current TWs to the right of that transition point (the total currents must satisfy Kirchhoff's current law).

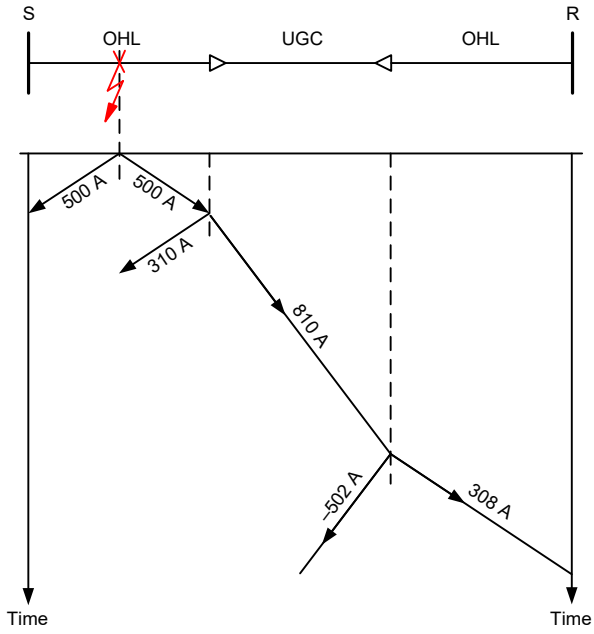

Fig. 12. Incident, reflected, and transmitted TWs for a fault on Section 1 of the hybrid line in Table I.

Note that the double-ended TW-based fault locator in this example has more than sufficient current TW signals to work with at both Terminals S and R, 500 A and 308 A incident TWs, respectively.

4) Numerical Example 2

Assume a fault on Section 2 of the hybrid line in Table I. Assume further, a bolted fault occurred when the voltage was at 150 kV peak, launching an incident current TW of 150 kV / 70 Ω = 2143 A. Fig. 13 shows the incident and reflected TWs for this fault neglecting any attenuation and dispersion.

Note that the double-ended TW-based fault locator in this example has more than sufficient current TW signals to work with at both terminals of the line (814 A incident TWs at both main line terminals despite the considerable TW signal reduction when transitioning from the cable Section 2 to the overhead Sections 1 and 3).

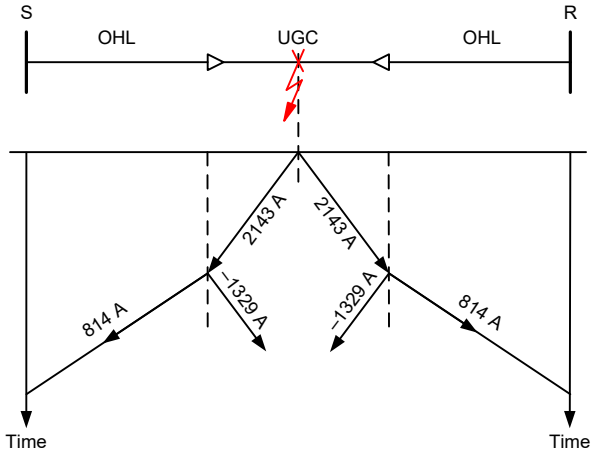

Fig. 13. Incident, reflected, and transmitted TWs for a fault on Section 2 of the hybrid line in Table I.

5) Numerical Example 3

Assume line energization from Terminal S at a time instant when the voltage was at 120 kV, launching a 120 kV / 300 Ω = 400 A incident current TW toward the remote terminal with an open circuit breaker. Fig. 14 shows the incident and reflected TWs for this event neglecting any attenuation and dispersion.

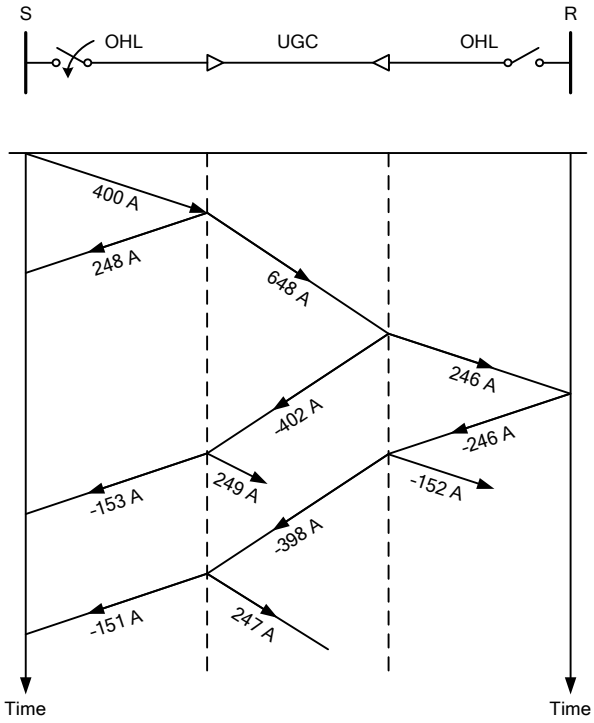

Fig. 14. Incident, reflected, and transmitted TWs for a line energization test of the hybrid line in Table I.

Note that the incident current TW signals returning to Terminal S are as follows:

- 248 A (or 62 percent of the launched TW) from the Section 1–2 transition.
- –153 A (or 38 percent of the launched TW) from the Section 2–3 transition.
- –151 A (or 38 percent of the launched TW) from the remote end of the line.

The actual TW magnitudes will be further reduced by attenuation in the cable sections.

Examples 1 and 2 show that for internal faults, the double-ended TW-based fault locator works with adequate first current TW signals. However, during the line energization test (Example 3), the TW launched by the circuit breaker closure travels a long distance and goes through multiple discontinuities, resulting in low-magnitude current TWs returning all the way back from the remote terminal to the energizing terminal. The next section elaborates on the line energization test for obtaining accurate TW fault locator settings and it proposes some solutions for better measurement of the TW line propagation times during energization of a hybrid line.

IV. Obtaining Configuration Data for Better Accuracy of the Traveling-Wave Fault Locator

As explained in Section III.B, line data (line length and TW line propagation time) impact fault-locating accuracy. This section teaches how to measure the TW line (or section) propagation time to improve fault-locating accuracy.

A. Two-Terminal Overhead Lines

When a power line is energized, the closure of the circuit breaker pole applies a voltage step to the de-energized conductor, and therefore, it launches a wave that travels to the remote terminal. Because the remote circuit breaker is open, the current TW reflects completely and arrives back at the local terminal with opposite polarity (see (9) and assume infinity as the impedance of the open line end). The TW travels twice the line length. Therefore, the time measured between the time the wave was launched and when it arrived back is twice the TW line propagation time.

For better fault-locating accuracy, measure the TW line propagation time using the line energization test. Apply the following best practices:

- The three circuit breaker poles exhibit a natural scatter when closing. If possible, use the last pole closure to measure the TW line propagation time so that the TW returning from the remote terminal arrives back at the local terminal when all three circuit breaker poles are already closed. This method produces the same TW modes as those produced during line faults.
- Estimate the TW arrival time from the remote terminal using a propagation velocity of about 98 percent of the speed of light in free space for overhead lines. Use this estimate to identify the correct TW as the first return from the remote terminal.
- Use a TW measured in a selected aerial mode (not a phase signal). Consider the mode with the highest magnitude and the cleanest shape (a step change with minimum dispersion and ringing). Typically, it is best to select the alpha aerial mode that corresponds with the last circuit breaker pole to close. The fault-locating solution described in [8] provides software to plot all modes from the phase signals in the recorded oscillography file.
- Use the same time-stamping method as your fault locator when measuring the propagation time. Otherwise your TW line propagation time can be slightly different when measured with an arbitrary time-stamping method versus when measured using your specific fault-locating method. The fault-locating solution described in [8] provides software to plot TWs as measured by the fault-locating device (the output from the differentiator-smoother filter).
- If possible, repeat the line energization test to double-check your result. Use test cases that created a large voltage step when closing the last pole of the circuit breaker. Consider energizing the line from the other terminal when validating your TW line propagation time measurements. You can also use the times measured using the closure of the first two circuit breaker poles to check your result. Remember that these times may be slightly different because the returning TWs arrive at the terminal with some circuit breaker poles still open, and therefore they exhibit different termination effects in the phases already closed compared with the phases still open.

B. Hybrid Lines

You can use the line energization test to measure the TW line propagation time for each section of a hybrid line. Each transition between an overhead line section and an underground cable section results in a TW reflection, i.e., a TW sent back to the energizing terminal (see Fig. 14). These reflections allow you to measure the TW line propagation times between the terminal and each significant discontinuity along the line in a manner similar to the TDR method.

Apply the following best practices when measuring the TW line propagation times for individual sections of a hybrid line:

- Estimate the arrival time for each transition point as twice the propagation time from the terminal to each transition point. Consult your cable data sheet, cable manufacturer, or your own present or historical TDR test results for a given cable type to estimate the propagation velocity for your cable sections.
- Because of high attenuation and dispersion, you may not be able to see reflections from transition points away from the energizing terminal. If so, perform tests from both ends of the line to identify reflections from transitions close to each of the respective terminals.
- An alternative solution is to pick up load at the remote terminal while measuring TWs at the local terminal. This way you will measure TWs that traveled a line length and not twice the line length, alleviating the attenuation problem by the factor of two. However, the magnitudes of TWs launched by picking up load may be lower compared with TWs from energizing the line, and this method may not guarantee the best outcome.
- Yet another solution is to energize the line multiple times, adding sections one at a time by closing disconnect links between the sections. This way, you

will measure reflections from an open section end instead of reflections from a discontinuity. Reflections from an open end are higher in magnitude than reflections from the transition between an overhead section and a cable section.

- Because of high dispersion in cables, always use the fault locator time-stamping method to measure the TW arrival times. A generic TDR measurement of the TW propagation time may be slightly different than the fault locator measurement depending on the TDR principle of operation.

C. Numerical Example

Consider a hybrid line as in Table I. Only the section length data in Table I is available to you prior to the energization test. Use the length data and assumed propagation velocity of 98 percent of the speed of light in free space for the overhead sections. For the type of cable comprising Section 2, assume your historical data show the TW propagation velocity to be about 55 percent of the speed of light in free space. Estimate the propagation time for each section as follows:

Overhead line, Section 1 propagation time:

$$\frac{20 \text{ mi}}{0.98 \cdot 186{,}282 \text{ mi/s}} = 110 \text{ µs}$$

Underground cable, Section 2 propagation time:

$$\frac{8 \text{ mi}}{0.55 \cdot 186{,}282 \text{ mi/s}} = 78 \text{ µs}$$

Overhead line, Section 3 propagation time:

$$\frac{10 \text{ mi}}{0.98 \cdot 186{,}282 \text{ mi/s}} = 55 \text{ µs}$$

When energizing the line from Terminal S, expect these TW arrival times from the line transition points:

- From the Section 1–2 transition, about 220 µs.
- From the Section 2–3 transition, about 376 µs.
- From the remote terminal (R), about 486 µs.

When energizing the line from Terminal R, expect these TW arrival times from the line transition points:

- From the Section 2–3 transition, about 110 µs.
- From the Section 1–2 transition, about 266 µs.
- From the remote terminal (S), about 486 µs.

Fig. 15 and Fig. 16 show the TW signals for line energization from Terminals S and R, respectively (compare with Fig. 14 to understand the timing, polarity, and magnitude of the TWs reflected from the discontinuities of the line). The top of each figure shows the phase currents, while the bottom is a magnification of the proper current alpha aerial mode TW. Table II shows the TW arrival time results. In both cases (energization from Terminals S and R), the Phase C pole of the circuit breaker closed last. Therefore, we plot the aerial alpha mode referenced to Phase C for measurement of the propagation times.

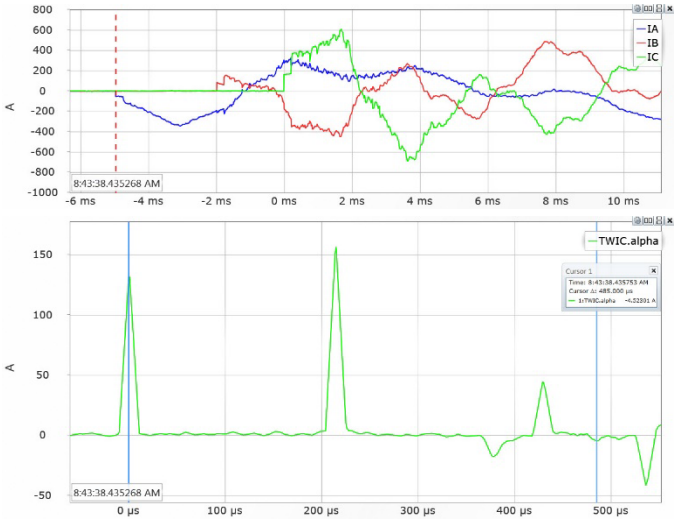

Fig. 15. Example of energizing the line in Table I from Terminal S. Reflections are recorded at 215, 378, and 485 µs following the TW launched by the Phase C pole closure. The second cursor identifies the reflection arriving at 485 µs.

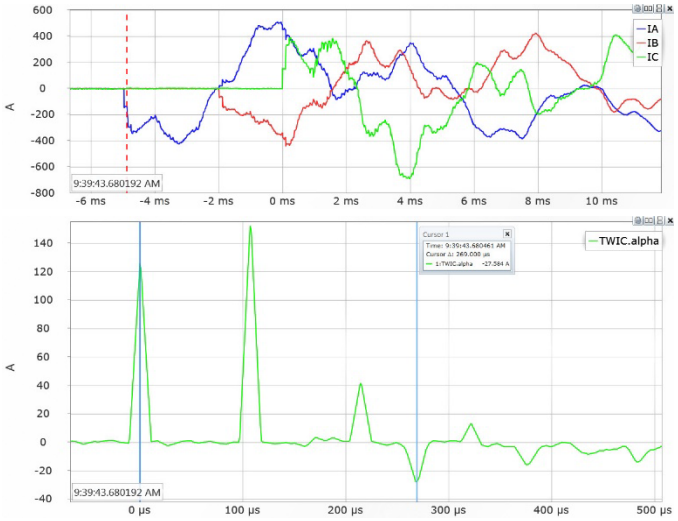

Fig. 16. Example of energizing the line in Table I from Terminal R. Reflections are recorded at 107, 269, and 484 µs following the TW launched by the Phase C pole closure. The second cursor identifies the reflection arriving at 269 µs.

TABLE II
PROPAGATION TIMES MEASURED DURING LINE ENERGIZATION

Section	Round Trip	Round Trip Time (µs)
Energizing from Terminal S		
1	From Terminal S to the Section 1–2 transition	215.0
1+2	From Terminal S to the Section 2–3 transition	378.0
1+2+3	From Terminal S to Terminal R	485.0
Energizing from Terminal R		
3	From Terminal R to the Section 2–3 transition	107.0
3+2	From Terminal R to the Section 1–2 transition	269.0
3+2+1	From Terminal R to Terminal S	484.0

Based on energization from Terminal S, we obtain these results:

- Section 1: $0.5 \cdot 215\ \mu s = 107.5\ \mu s$
- Section 2: $0.5 \cdot (378 - 215)\ \mu s = 81.5\ \mu s$
- Section 3: $0.5 \cdot (485 - 378)\ \mu s = 53.5\ \mu s$

Based on energization from Terminal R, we obtain these results:

- Section 3: $0.5 \cdot 107\ \mu s = 53.5\ \mu s$
- Section 2: $0.5 \cdot (269 - 107)\ \mu s = 81.0\ \mu s$
- Section 1: $0.5 \cdot (484 - 269)\ \mu s = 107.5\ \mu s$

Note that when energizing the line from Terminal S, we obtained slightly different values of the section TW line propagation times than when energizing the line from Terminal R. We explain this effect by different line dispersion and attenuation as seen from one terminal versus the other (different distance traveled by the TWs). For example, when measuring the Section 3 time by energizing from Terminal S, we measure time stamps from TWs that traveled a longer distance and became reduced in magnitude because they went through two discontinuities before reaching Section 3. When measuring the Section 3 time by energizing from Terminal R, we work with TWs that originated from the circuit breaker without going through any extra transitions and are less dispersed because they traveled a shorter distance when they reached the Section 2–3 transition point.

You can average the results from multiple tests. Consider giving priority to measurements obtained from TWs that traveled a shorter distance. In our example, use energization from Terminal S to obtain Section 1 data, energization from Terminal R to obtain Section 3 data, and the average to obtain Section 2 data as follows:

- Section 1 TWLPT = 107.5 μs (measured from S)
- Section 3 TWLPT = 53.5 μs (measured from R)
- Section 2 TWLPT = $0.5 \cdot (81.5 + 81.0)\ \mu s = 81.25\ \mu s$

In this example, we read the time stamps visually from the plot. We set the fault locator as in Table I using slightly more accurate time stamps with submicrosecond resolution, obtained using interpolation and through averaging results from multiple energization tests. Note that the differences are very small, around a quarter of a microsecond.

V. Adaptive Autoreclosing Control Logic

In reference to Fig. 17, an adaptive autoreclosing logic provides settings that allow the user to specify multiple blocking regions for autoreclosing. The logic asserts an output bit a few milliseconds after the fault if the calculated fault location falls in any of the blocking regions. Apply this blocking bit as follows:

- Use this bit in your autoreclosing scheme to cancel reclosing.
- In single-pole tripping applications, use this bit to force three-pole tripping for single-line-to-ground (SLG) faults. This way a line-protection scheme trips a single pole of a breaker and recloses for a SLG fault on an overhead section, but the scheme trips three poles for a SLG fault on a cable section without reclosing.

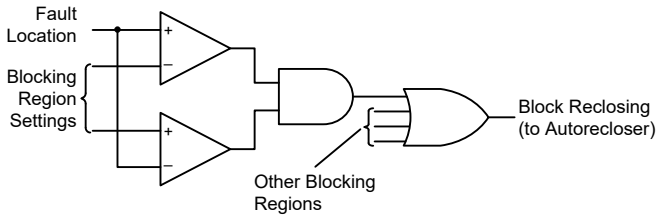

Fig. 17. Simplified autoreclosing control logic.

Apply margin when setting the blocking regions to avoid spurious reclosing onto cable faults or onto faults located in the "do not reclose" zones in other applications. Set the blocking region slightly longer than the "do not reclose" stretch of the line. Consult the manufacturer's fault-locating accuracy specification when selecting margins.

The adaptive autoreclosing control logic may provide a setting to decide if autoreclosing shall be allowed or canceled if the fault-locating algorithm fails to locate the fault for any reason. If the fault location information is missing, the logic may block or allow autoreclosing based on the default output setting. In applications to hybrid lines, you may decide to block reclosing for the entire line if the fault location is not available. In other applications, you may decide to allow or to block reclosing for all line faults depending on your preferences for that specific application.

VI. Conclusions

In this paper, we discussed the benefits of using fault location to adaptively control autoreclosing for power lines—to allow reclosing for some fault locations and to prevent reclosing for other fault locations along the line. These applications include blocking autoreclosing for line sections in fire-prone rural terrains, near small airports, or in densely populated urban areas.

Blocking reclosing for faults in cable sections of hybrid lines comprising overhead line sections and underground cable sections is the prime application for the adaptive, location-dependent reclosing. Impedance-based fault locators are not sufficiently accurate to support location-dependent reclosing for hybrid lines. Installing CTs and associated measuring devices at the overhead-to-cable transition points and using fiber-optic communications to collect current values at the line terminal where the autoreclosing device is located allows creating differential zones that discriminate cable faults from overhead faults. However, this solution is expensive and complicated.

This paper explains how to extend the original double-ended TW-based fault-locating method derived for homogeneous lines, to hybrid lines in which the cable and overhead sections have different TW propagation velocities. The method is simple to implement and apply. It requires time synchronization and communications, but only between the main terminals of the line and not between the terminals and each overhead-to-cable

transition point. It has accuracy on the order of 300 m (1000 ft) for faults on overhead line sections, and 150 m (500 ft) for faults on cable sections.

The paper presents operation examples from the double-ended TW-based fault locator integrated with an adaptive autoreclosing control logic implemented in a relay [8].

Performing line energization tests is a recommended practice to obtain accurate settings for the TW-based fault locator. Using operational data after the initial commissioning of the fault locator allows further fine-tuning of the application for even better accuracy. The paper explains the principles and provides numerical examples of such fine-tuning using operational data.

VII. Appendix. Improving Fault-Locating Performance Based on Field Data

In Section IV, we explained how to measure the line (or line section) TW propagation time for better accuracy of TW-based fault locating. Note that the line (or line section) TW propagation time is an unambiguous and directly measurable parameter. We cannot say the same about the line length. Line length is much more ambiguous and cannot be easily measured. Moreover, a typical approach to measuring the length of electrical conductors is to use the TDR method to measure the TW propagation time along the conductors, only to convert it into length assuming a certain TW propagation velocity.

Fig. A.1 illustrates the line length ambiguity by depicting four different definitions of distance between two adjacent towers:

- d_1 is the length of the power conductors, which depends on their sag and may change with ambient temperature and line loading. This distance is probably the most accurate measure of the distance TWs travel.
- d_2 is the straight-line distance between the insulators. This distance is fixed and partially reflects the terrain elevation, but it neglects the conductor sag.
- d_3 is the distance between the towers neglecting terrain elevation. This distance may be the easiest to measure from two-dimensional mapping data.
- d_4 is the actual distance between towers measured on the terrain surface. This distance may be the most accurate measure of the distance for a foot patrol, but is not a practical distance measure for a line crew in today's world.

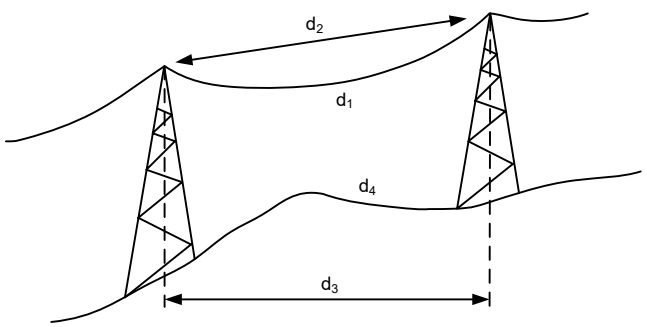

Fig. A.1. Four different definitions of length for an overhead power line.

None of the above methods of defining distance solves the challenge of converting the $t_S - t_R$ time measurement in the fundamental fault-locating equation (4) into a very precise fault location in the three-dimensional physical world. Note that with a precise $t_S - t_R$ time measurement and a precise TWLPT setting, (4) provides an exceptionally accurate per-unit fault location:

$$m = \frac{1}{2} \cdot \left(1 + \frac{t_S - t_R}{TWLPT}\right) \tag{A.1}$$

If we simply multiply the above precise number by the total line length as we know it, we may actually degrade the accuracy of the fault location value due to the inherent ambiguity in the line length data. This section offers some thoughts on how to improve fault-locating accuracy using operational data after putting the fault locator in service.

A. Refining Fault-Locating Settings

1) External Faults and Switching Events

External faults and switching events launch TWs that pass through the power line. If we set the fault-locating device oscillography to trigger from TW disturbance detectors, we will capture time-synchronized records at both line terminals. By comparing time stamps for such external events at both ends of the line, we have a chance to refine the TW line propagation time setting. Such measurements allow us to verify the initial TW line propagation time setting and to obtain a more accurate measurement for a particular sag on the line. This way we gain knowledge about the relationship between the ambient temperature, line loading, and the TWLPT setting for the fault locator. We can correct the result obtained from the fault locator (M_{FL}) (commissioned with a $TWLPT_{SET}$ setting) to get a more accurate value of the $TWLPT_{PRESENT}$ setting by solving (4) as follows:

$$M = \frac{LL}{2}\left[1 + \left(\frac{2 \cdot M_{FL}}{LL} - 1\right)\frac{TWLPT_{SET}}{TWLPT_{PRESENT}}\right] \tag{A.2}$$

For example, assume the fault locator commissioned with TWLPT = 536 μs on a 100 mi line reported the fault location as 56.345 mi. Your records indicate that given the ambient temperature and the line loading, 538 μs was a more accurate TW line propagation time for that fault. In your SCADA software, you can correct the original result from the fault locator using (A.2) and obtain 56.321 mi as a more accurate value. The difference is relatively small in this example (127 ft), but even a small difference can result in sending the line crew to an adjacent tower rather than the correct one.

2) Internal Faults

A number of factors can cause a small discrepancy between the fault location reported by the fault locator and the location confirmed by the line crew. Always try to verify the TWLPT and the LL settings first. Assume you collected data for several (more than two) internal faults and have a set of reported (M_{FL}) and confirmed or actual (M_{ACT}) fault locations for each case. You can run a least errors square algorithm to find the TWLPT and LL values that would minimize the fault-locating error for all your historical cases. To do this, first calculate the TW

arrival time difference for each case, solving (4) for the TW arrival time difference while using the TWLPT and LL settings as left in the fault-locating device at commissioning:

$$\Delta t = t_S - t_R = TWLPT \cdot \left(\frac{2 \cdot M_{FL}}{LL} - 1\right) \qquad (A.3)$$

Your TWLPT and LL settings applied in the fault locator are relatively accurate. Assume 0.3 percent error in the TWLPT setting (sag) and 2 percent error in the LL setting, and perform a numerical search around TWLPT ± 0.3 percent and LL ± 2 percent. Look for a pair of TWLPT and LL settings that would minimize the fault-locating error across all cases. In effect, you attempt to minimize this expression:

$$\sum\nolimits_k \left[M_{ACT(k)} - \frac{LL}{2} \cdot \left(1 + \frac{\Delta t_{(k)}}{TWLPT}\right)\right]^2 \qquad (A.4)$$

For example, assume the fault locator commissioned to use TWLPT = 548 μs on a 100 mi line reported several fault locations in the past for which the line crew found and confirmed faults. Table A.I shows the actual fault locations, the original fault locations and errors, and the fault locations and errors obtained using updated (fine-tuned) TWLPT and LL settings.

TABLE A.I
FAULT LOCATION AND ERROR VALUES OBTAINED USING THE ORIGINAL SETTINGS, AND USING SETTINGS REFINED BY FITTING NEW TWLPT AND LL DATA TO HISTORICAL CASES

Fault No.	M_{ACT} (mi)	Original Settings		Refined Settings	
		M_{FL} (mi)	Error (mi)	M_{FL} (mi)	Error (mi)
1	23.254	23.514	–0.260	23.278	–0.024
2	56.521	56.689	–0.168	56.473	0.048
3	13.554	13.858	–0.304	13.616	–0.062
4	78.173	78.279	–0.106	78.076	0.097
5	88.564	88.856	–0.292	88.6593	–0.095

The refined settings are 545.26 μs (instead of 548 μs) and 99.56 mi (instead of 100 mi), respectively. These new settings reduce the total error squared from 0.2843 mi^2 to 0.0252 mi^2 for all five cases in Table A.I.

This approach is especially helpful if you have systemic errors in the reported fault location, such as when actual fault location is consistently short of the reported location, as in the example in Table A.I. Such systemic errors tend to indicate errors in the settings, especially the line length.

Of course, if your new line length and TW line propagation time yield the propagation velocity that is higher or considerably lower than the speed of light in free space, you need to check your input data for accuracy.

B. Refining the Mapping of Fault Location Into Tower Positions

Another practical solution for improving accuracy of the information given to the line crews looking for line faults is to develop a more accurate mapping between a fault location as calculated by the fault locator and an identification tag of the tower with the fault. This mapping is effectively a mapping between the linear distance-to-fault indication and the geospatial tower locations, i.e., GPS coordinates of line towers. This mapping can be programmed as a post-processing task in your SCADA software. Fig. A.2 illustrates such mapping.

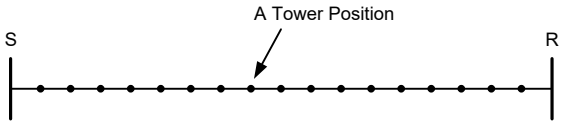

Fig. A.2. An example of mapping distance to fault into tower locations.

Initially, you may place markers representing line towers based on the nominal distance of each tower from the line terminals. We can refine these positions using internal fault data as follows.

If the fault locator reported a distance of M_1 for a line fault, while the line crew found the fault at a tower nominally located at M_0 on the one-dimensional line graph, and M_0 and M_1 are relatively close, consider "repositioning" this tower from M_0 to a new location closer to the confirmed location of M_1. Use (A.5) to calculate the new tower position:

$$M_{0(NEW)} = M_{0(OLD)} + \alpha \cdot \left(M_1 - M_{0(OLD)}\right) \qquad (A.5)$$

where α is a learning coefficient between 0 (no learning) and 1 (very aggressive learning).

For example, with α = 0.25, reposition the tower by one quarter of the distance between the old position and the new position corresponding to the confirmed fault location.

Once a given tower has been effectively repositioned from the previously known position to a new position confirmed by a fault locator, consider proportionally repositioning all other towers between the tower in question and the nearest confirmed location (another fault-confirmed tower, a line terminal, or a line tap). The following numerical example illustrates this approach.

Assume a double-ended TW-based fault locator reported a fault at 10.935 mi and the line crew found the fault at the tower located at 11.054 mi, as per the present tower position table. Assuming a learning coefficient of 0.5, you may calculate the updated position of that tower to be:

$$10.935 + 0.5 \cdot (11.054 - 10.935) = 10.995 \text{ mi}$$

Assume further that the nearest confirmed location to that tower is the local terminal. If so, consider updating all the tower positions located between that tower and the local terminal. In one approach, divide the small correction you applied to the tower in question among all the tower spans between the tower in question and the line terminal. In another approach, reposition one tower and leave the other towers at their nominal positions. In yet another approach, reposition all the towers proportionally to their distance from the line terminal, i.e., by multiplying them by 10.995/11.054 or 0.99466 in this example. You may update the positions of all the towers toward the other

terminal accordingly using one of the three approaches outlined above.

Table A.II shows the related fragment of the tower position table for this numerical example. The tower positions in the table have been multiplied by a constant that reflects the change in the position of Tower L23-60. This way, towers close to Tower L23-60 are repositioned more than the towers away from Tower L23-60. Towers close to the line terminals are practically left at their nominal positions. In other words, all towers are repositioned by the same small fraction of their distance to the terminal.

TABLE A.II
ORIGINAL AND REFINED TOWER POSITION EXAMPLE

Tower ID	GPS Coordinates	Tower Position	
		Original (mi)	Refined (mi)
L23-58	X° Y′ Z″ N/S X° Y′ Z″ W/E	10.664	10.607
L23-59	X° Y′ Z″ N/S X° Y′ Z″ W/E	10.864	10.806
L23-60	X° Y′ Z″ N/S X° Y′ Z″ W/E	11.054	10.995
L23-61	X° Y′ Z″ N/S X° Y′ Z″ W/E	11.224	11.169
L23-62	X° Y′ Z″ N/S X° Y′ Z″ W/E	11.424	11.129

Following this approach, you will improve the accuracy of the information provided to line crews after the first few faults have been correctly located on the line and used to adjust the mapping between the reported fault (and thus tower) location and the positions of the towers in your tower position table.

Use this approach only after making sure the TW line propagation time and the total line length settings are accurate. You should not use faults reported by the fault locator with a relatively large error to improve the accuracy of your tower locations.

VIII. REFERENCES

[1] E. O. Schweitzer, III, "A Review of Impedance-Based Fault Locating Experience," proceedings of the 43rd Annual Georgia Tech Protective Relaying Conference, Atlanta, GA, May 1989.

[2] C37.104-2002 – IEEE Guide for Automatic Reclosing of Line Circuit Breakers for AC Distribution and Transmission Lines.

[3] P. Orr, G. Fusiek, C. D. Booth, P. Niewczas, A. Dysko, F. Kawano, P. Beaumont, and T. Nishida, "Flexible Protection Architectures Using Distributed Optical Sensors," proceedings of the 11th IET International Conference on Developments in Power System Protection, Birmingham, UK, April 2012.

[4] A. Abolins, D. Lambrecht, J. S. Joyce, and L. T. Rosenberg, "Effect of Clearing Short Circuit and Automatic Reclosing on Torsional Stress and Life Expenditure of Turbine Generator Shafts," IEEE Trans. PAS, Vol. PAS-95, No. 1, 1976, pp. 14–85.

[5] D. Tziouvaras, "Protection of High-Voltage AC Cables," proceedings of the 32nd Annual Western Protective Relay Conference, Spokane, WA, October 2005.

[6] Y. Gong, M. Mynam, A. Guzmán, G. Benmouyal, and B. Shulim, "Automated Fault Location System for Nonhomogeneous Transmission Networks," proceedings of the 65th Annual Conference for Protective Relay Engineers, College Station, TX, April 2012.

[7] J. Vargas, A. Guzmán, and J. Robles, "Underground/Submarine Cable Protection Using a Negative-Sequence Directional Comparison Scheme," proceedings of the 26th Annual Western Protective Relay Conference, Spokane, WA, October 1999.

[8] SEL-T400L Time-Domain Line Protection Instruction Manual. Available: https://selinc.com.

[9] E. O. Schweitzer, III, A. Guzmán, M. V. Mynam, V. Skendzic, B. Kasztenny, and S. Marx, "Locating Faults by the Traveling Waves They Launch," proceedings of the 40th Annual Western Protective Relay Conference, Spokane, WA, October 2013.

[10] SEL-411L Advanced Line Differential Protection, Automation, and Control System Instruction Manual. Available: https://selinc.com.

IX. BIOGRAPHIES

Bogdan Kasztenny has specialized and worked in power system protection and control since 1989. In his decade-long academic career, Dr. Kasztenny taught power system and signal processing courses at several universities and conducted applied research for several relay manufacturers. Since 1999, Bogdan has designed, applied, and supported protection, control, and fault locating products with their global installed base counted in thousands of installations. Since 2009, Bogdan has been with Schweitzer Engineering Laboratories, Inc. where he works on product research and development. Bogdan is an IEEE Fellow, a Senior Fulbright Fellow, a Canadian representative of the CIGRE Study Committee B5, and a registered professional engineer in the province of Ontario. Bogdan has served on the Western Protective Relay Conference Program Committee since 2011 and on the Developments in Power System Protection Conference Program Committee since 2015. Bogdan has authored over 200 technical papers and holds over 30 patents.

Armando Guzmán received his BSEE with honors from Guadalajara Autonomous University (UAG), Mexico. He received a diploma in fiber-optics engineering from Monterrey Institute of Technology and Advanced Studies (ITESM), Mexico, and his master of science and PhD in electrical engineering and masters in computer engineering from the University of Idaho, USA. He served as regional supervisor of the Protection Department in the Western Transmission Region of the Federal Electricity Commission (the electrical utility company of Mexico) in Guadalajara, Mexico for 13 years. He lectured at UAG and the University of Idaho in power system protection and power system stability. Since 1993 he has been with Schweitzer Engineering Laboratories, Inc. in Pullman, Washington, where he is a fellow research engineer. He holds numerous patents in power system protection and metering. He is a senior member of IEEE.

Mangapathirao (Venkat) Mynam received his MSEE from the University of Idaho in 2003 and his BE in electrical and electronics engineering from Andhra University College of Engineering, India, in 2000. He joined Schweitzer Engineering Laboratories, Inc. (SEL) in 2003 as an associate protection engineer in the engineering services division. He is presently working as a senior research engineer in SEL research and development. He was selected to participate in the U. S. National Academy of Engineering (NAE) 15th Annual U. S. Frontiers of Engineering Symposium. He is a senior member of IEEE and holds eight patents in the areas of power system protection, control, and fault location.

Titiksha Joshi is a Power Engineer in the Research group of Schweitzer Engineering Laboratories, Inc. She received her bachelor's degree in electrical engineering from Mumbai University, India in 2012 and a master of science degree in electrical engineering from Arizona State University in 2014. She has worked as an intern at Crompton Greaves (2011) and Midcontinent Independent System Operator, Inc. (2013).

Previously presented at the 2018 Texas A&M Conference for Protective Relay Engineers.

20191009 • TP6820-01